Two-Layer Models of Abyssal Equator-Crossing Flow

PAUL F. CHOBOTER

College of Oceanic and Atmospheric Sciences, Oregon State University, Corvallis, Oregon

GORDON E. SWATERS

Applied Mathematics Institute, Department of Mathematical and Statistical Sciences, and Institute for Geophysical Research, University of Alberta, Edmonton, Canada

(Manuscript received 28 August 2002, in final form 16 December 2002)

ABSTRACT

The role of baroclinicity in the dynamics of abyssal equator-crossing flows is examined by studying two-layer models of the flow valid in the equatorial region. Three new analytical models are derived from two-layer shallow-water theory. One of these models (Equatorial Model I, or EMI) reduces to the Swaters and Flierl coupled model in the midlatitude limit. In the equatorial limit, the lower-layer dynamics of EMI are that of the complete shallow-water equations, and the upper-layer dynamics are built upon quasigeostrophic potential vorticity conservation with a balance equation to relate the streamfunction and pressure. Simple numerical simulations are performed using this model to investigate its behavior in certain idealized situations, including equator-crossing lenses and currents. In the midlatitudes, the dynamics of EMI are characterized by strong baroclinic interactions between the layers, while near the equator all three models exhibit a partial decoupling of the layers. This motivates the use of a one-layer reduced-gravity model to simulate abyssal dynamics in the immediate vicinity of the equator. Such simulations are reported elsewhere. A uniformly valid metamodel is derived that contains all of the necessary terms so that it may reduce, in the appropriate parameter limit, to any of the three models derived here.

1. Introduction

Observations of deep western boundary currents (DWBCs) approaching and crossing the equator exist in the Atlantic, Pacific, and Indian Oceans. In the Atlantic, Antarctic Bottom Water (AABW) flows northward along the western slope of the Brazil Basin (DeMadron and Weatherly 1994), northeast through a channel at the equator (Rhein et al. 1995; Hall et al. 1997), and into the North Atlantic, where it flows along the western slope of the Mid-Atlantic Ridge (Friedrichs and Hall 1993). Not all of the AABW crosses the equator: it seems to split into two currents partway through the Brazil Basin, and only the less dense branch flows into the equatorial channel (Sandoval and Weatherly 2001). In the Pacific, Lower Circumpolar Water flows northward as a DWBC through the Samoan Passage at 10°S (Roemmich et al. 1996; Rudnick 1997), and there is evidence of these waters at 10°N (Johnson and Toole 1993; Wijffels et al. 1996). In the Indian Ocean, Lower Circumpolar Water flows northward as a DWBC along the western slope of the Somali Basin and appears to turn eastward at the equator (Johnson et al. 1991). Some of this fluid is known to exit the Somali Basin through the Owen Fracture Zone near the north end of the basin at 11°N (Quadfasel et al. 1997).

The dynamics of these abyssal cross-equatorial flows are not completely understood. Stommel and Arons (1972) studied DWBCs using an inertial analytical model of a current flowing over a sloping bottom at midlatitudes, assuming the potential vorticity of the flow to be conserved. This model was extended by Johnson (1993) to be valid on an equatorial β plane, and the analytical solution was used to study the features of a DWBC that crossed the equator while conserving its potential vorticity. The same model has been generalized to account for cross-stream variations of potential vorticity (Pickart and Huang 1995), though the application was restricted to midlatitudes. Nof and Borisov (1998) argue that the effects of friction, bottom topography, and inertia are all important in the equator-crossing process, and used reduced-gravity shallow water simulations to study equator-crossing flow over idealized topography (see also Borisov and Nof 1998).

One aspect of the dynamics that has received little attention is how these currents dynamically couple with the overlying fluid. This may be addressed in a prelim-

Corresponding author address: Prof. Gordon E. Swaters, Department of Mathematical and Statistical Sciences, University of Alberta, Edmonton, AB T6G 2G1, Canada.
E-mail: Gordon.Swaters@ualberta.ca

inary way by studying a two-layer model of the flow. It is desirable for a two-layer equatorial model to reduce to the appropriate geostrophically balanced model in the midlatitude limit. Karsten and Swaters (1999) derived and classified all the possible frontal geostrophic models derivable from two-layer shallow-water theory, and found that the appropriate one for the case in which the lower layer is thin compared to the overlying water column and the bottom topography plays an important dynamical role is the model derived by Swaters and Flierl (1991).

The Swaters and Flierl model captures the baroclinic, subinertial dynamics of a thin lower layer flowing over bottom topography coupled to a thick upper layer in which the flow is geostrophic to leading order. The model is derived from two-layer shallow-water theory by an asymptotic expansion in terms of a parameter that plays the role of the Rossby number of the flow (Swaters 1991; Swaters and Flierl 1991). The resulting dynamics may be thought of as being modeled by planetary geostrophy in the lower layer and quasigeostrophy in the upper layer, with a coupling between the pressure fields of the two layers.

However, the model of Swaters and Flierl (1991) cannot be used near the equator because it was derived under the f-plane approximation with geostrophy holding at leading order. That is, dynamics arising from the meridional variation of the Coriolis parameter are neglected and, in particular, the Coriolis parameter is not permitted to be zero. This is a reasonable approximation at midlatitudes and on small enough length scales, but not if the domain includes the equator. One of the goals of this work is to investigate to what extent the Swaters and Flierl model may be extended to the equator. In other words, can a model be developed that captures the dynamics of these equator-crossing currents and that simplifies, in the midlatitude limit, to the Swaters and Flierl model?

We will show that such a model can, in fact, be derived, provided that the geostrophic balance relation is generalized to a relation describing well-defined velocities in the equatorial limit. We will employ two such generalizations, each valid only for its respective layer. While neither relation is individually new, they have not, to our knowledge, previously been written down *together* to form a coupled two-layer model applicable at the equator.

The generalization to the geostrophic relation used in the upper layer is similar to the Charney balance equations studied, for example, by Gent and McWilliams (1983). The generalization used in the lower layer is, depending on the relative sizes of certain parameters, either the reintroduction of inertial terms or a three-way balance among the pressure gradient, the Coriolis effect, and friction. The difference between an equatorial model driven by inertial effects and one driven by frictional effects is studied by Choboter and Swaters (2002, manuscript submitted to *J. Phys. Oceanogr.*, hereinafter CS02). They point out that the frictional model does not permit upslope flow under any circumstances. We will show, via an extension of the Nof (1983, hereinafter referred to as N83) analysis for the translation velocity of abyssal domes along a sloping bottom in midlatitudes, that the introduction of an upper layer, that is, baroclinic dynamics, may relax that restriction.

In section 2 the N83 derivation is generalized to include the effects of the upper layer and friction. In section 3, the model representing the extension of the Swaters and Flierl (1991) model to the equator is derived and numerical simulations are presented to display its behavior. In section 4, alternate models of equatorial flow are derived, and a metamodel is described in section 5 that simplifies to each of the previously derived models in the appropriate limits. A summary is given in section 6.

2. Effect of upper layer and friction on abyssal lenses

Nof (1983) derived the velocity of a steadily traveling local mass of inviscid shallow water on a linearly sloping bottom on an f plane. This velocity is directed along the slope with speed $g's/f$, where g' is the reduced gravity, s is the slope of the bottom topography, and f is the Coriolis parameter. Swaters and Flierl (1991) modified the derivation of N83 to include the effects of baroclinic interactions with the upper layer. Here, we extend the analysis further to include the effects of bottom friction as parameterized by a linear damping term. This form of friction parameterizes the effects of a bottom Ekman layer since it acts as a vorticity sink proportional to the local relative vorticity, and therefore has the same effect on the vorticity dynamics as Ekman pumping (Pedlosky 1987).

A model employing such a linear damping term may be used to generalize the geostrophic relations to a three-way balance among the pressure gradient, the Coriolis force, and friction. This relation predicts well-defined flow at the equator and, indeed, has been used to study abyssal cross-equatorial flow (Stephens and Marshall 2000; CS02). However, such a model does not permit upslope mass flux, which is a severe restriction of the dynamics (CS02). As the following demonstrates, the addition of a dynamically active upper layer reintroduces the possibility of upslope flow back into the model.

In the context of two-layer shallow water flow, the equations of motion for the lower or abyssal layer, including the effects of variation in pressure of the upper layer and linear damping, may be written (see Fig. 1 for the geometry of the problem) as

$$\mathbf{u}_t + \mathbf{u}\cdot\nabla\mathbf{u} + f\hat{\mathbf{e}}_3\times\mathbf{u} + g'\nabla(h - sy) + g\nabla\eta = -r\mathbf{u}, \tag{2.1}$$

$$h_t + \nabla\cdot(\mathbf{u}h) = 0, \tag{2.2}$$

where $\mathbf{u}$ is the lower-layer velocity, $\nabla = (\partial_x, \partial_y)$, h is the lower-layer thickness, η is the upper-layer pressure, r is a damping coefficient, g is the gravitational acceleration, and g' is the reduced gravity. The bottom topography is assumed to be of the form $-sy$, where $s > 0$ is the slope of the topography. The rigid-lid approximation has been employed in the upper layer.

Let the region of nonzero layer thickness h have finite horizontal extent. Denote the region in the (x, y) plane of nonzero thickness by R and let the boundary of the region, ∂R, be given by $\phi(x, y, t) = 0$. On ∂R, the following boundary conditions apply:

$$\phi_t + \mathbf{u} \cdot \nabla\phi = 0; \qquad h = 0. \tag{2.3}$$

We assume that the dome of fluid is traveling steadily with velocity $\mathbf{c} = (c_x, c_y)$, and rewrite the equations in the comoving frame of reference. Let

$$\xi = x - c_x t, \qquad \zeta = y - c_y t \tag{2.4}$$

define the moving coordinates. Then the equations and boundary conditions in the moving frame of reference are

$$(\mathbf{u} - \mathbf{c}) \cdot \nabla\mathbf{u} + f\hat{\mathbf{e}}_3 \times \mathbf{u} + g'\nabla(h - sy) + g\nabla\eta = -r\mathbf{u}, \tag{2.5}$$

$$\nabla \cdot [(\mathbf{u} - \mathbf{c})h] = 0, \tag{2.6}$$

$$(\mathbf{u} - \mathbf{c}) \cdot \nabla\phi = 0 \quad \text{on } \phi(\xi, \zeta) = 0, \tag{2.7}$$

where we have used $\nabla \cdot \mathbf{c} = 0$. It has also been assumed that the upper-layer pressure η is steady in the comoving frame of reference, which will not hold in general if there is cross-slope motion because of the change in upper-layer thickness. This analysis therefore applies only in the limit of large upper-layer thickness and gently sloping bottom, in the sense made precise in section 3 where the equations are nondimensionalized. We may determine the steady velocity $\mathbf{c}$ by multiplying (2.5) by h and integrating over R, yielding

$$\int_R [h(\mathbf{u} - \mathbf{c}) \cdot \nabla\mathbf{u} + hf\hat{\mathbf{e}}_3 \times \mathbf{u} + hg'\nabla(h - sy) + hg\nabla\eta + hr\mathbf{u}]\, dA = \mathbf{0}. \tag{2.8}$$

Let us simplify this equation term by term. Note that the nonlinear advection term vanishes since

$$\int_R h(\mathbf{u} - \mathbf{c}) \cdot \nabla\mathbf{u}\, dA = \int_{\partial R} [h(\mathbf{u} - \mathbf{c}) \cdot \mathbf{n}]\mathbf{u}\, dl - \int_R \nabla \cdot [h(\mathbf{u} - \mathbf{c})]\mathbf{u}\, dA = \mathbf{0}.$$

The term proportional to g' may also be simplified as follows:

$$\begin{aligned}\int_R g'h\nabla(h - sy)\, dA &= -\hat{\mathbf{e}}_2 g's \int_R h\, dA + \frac{g'}{2}\int_R \nabla(h^2)\, dA \\ &= -\hat{\mathbf{e}}_2 g's \int_R h\, dA.\end{aligned}$$

To simplify the second and fifth terms in (2.8), note that the fact that the mass flux in the moving frame is horizontally nondivergent (2.6) implies that a mass transport streamfunction ψ exists such that $\hat{\mathbf{e}}_3 \times \nabla\psi = (\mathbf{u} - \mathbf{c})h$. Thus,

$$\begin{aligned}\int_R \mathbf{u}h\, dA &= \int_R \mathbf{c}h\, dA + \int_R \hat{\mathbf{e}}_3 \times \nabla\psi\, dA \\ &= \mathbf{c}\int_R h\, dA + \hat{\mathbf{e}}_3 \times \int_{\partial R} \psi\hat{\mathbf{n}}\, dl \\ &= \mathbf{c}\int_R h\, dA,\end{aligned}$$

where the second integral vanishes because ψ is constant on ∂R, which is true since on $\phi = 0$, $0 = h(\mathbf{u} - \mathbf{c}) \cdot \nabla\phi(\hat{\mathbf{e}}_3 \times \nabla\psi) \cdot \nabla\phi = J(\psi, \phi)$. Using this in (2.8) simplifies it to

$$f\hat{\mathbf{e}}_3 \times \mathbf{c} + r\mathbf{c} = g's\hat{\mathbf{e}}_2 - g\langle h\nabla\eta\rangle,$$

where $\langle(*)\rangle = \int_R (*)\, dA/\int_R h\, dA$.

The translation velocity $\mathbf{c}$ may be solved for

$$\mathbf{c} = \frac{r}{r^2 + f^2}\{g's\hat{\mathbf{e}}_2 - g\langle h\nabla\eta\rangle\} + \frac{f}{r^2 + f^2}\{g's\hat{\mathbf{e}}_1 + g\hat{\mathbf{e}}_3 \times \langle h\nabla\eta\rangle\} \tag{2.9}$$

or, componentwise,

$$c_x = \frac{f\{g's - g\langle h\eta_y\rangle\} - rg\langle h\eta_x\rangle}{f^2 + r^2}, \tag{2.10}$$

$$c_y = \frac{fg\langle h\eta_x\rangle + r\{g's - g\langle h\eta_y\rangle\}}{f^2 + r^2}. \tag{2.11}$$

Equation (2.9), or the pair (2.10) and (2.11), is the N83 along-slope velocity modified to include the effects of upper-layer pressure and lower-layer friction.

Some special cases may be investigated. In the limit as $\eta \to 0$ and $r \to 0$, Eq. (2.9) reduces to the N83 result describing along-slope motion with velocity $g's/f$. If only $r \to 0$, (2.9) reduces to the Swaters and Flierl (1991) result in which the along-slope velocity is modified to include the effects of the upper-layer pressure,

$$c_x = \frac{g's}{f} - \frac{g}{f}\langle h\eta_y\rangle, \qquad c_y = \frac{g}{f}\langle h\eta_x\rangle.$$

In the limit as $\eta \to 0$ with $r > 0$, (2.9) recovers the fact that the addition of friction to a simple geostrophic balance induces a downslope component to the flow,

$$\mathbf{c} = \frac{g's}{r^2 + f^2}(r\hat{\mathbf{e}}_2 + f\hat{\mathbf{e}}_1).$$

Note that an alternate derivation may be used to arrive at this particular result. The alternate derivation requires the assumption that a fluid parcel is moving along a slope in such a way that there exists a three-way balance among the forces of gravity, Rayleigh friction, and the Coriolis effect. Since such a derivation may be applied to any fluid parcel in such a balance, the result generalizes to currents in balance in addition to steady-traveling eddies (Reszka et al. 2002).

Clearly, the presence of a dynamically active upper layer modifies the direction of flow of the lower layer. In particular, note that it is possible, in principle, for the lower layer to induce an upslope component to the velocity, which is impossible in the simple model of abyssal flow studied by CS02 and employed for the study of abyssal cross-equatorial flow by Stephens and Marshall (2000).

3. Derivation from midlatitude scales

a. Generic nondimensionalization

We seek to model abyssal flow, taking into account interactions with the fluid above. From the outset, then, it is assumed that the lower layer is thin and the upper layer is relatively thick. The two-layer shallow-water equations may be written in dimensional form as

$$\mathbf{u}^*_{1t^*} + \mathbf{u}^*_1 \cdot \nabla^* \mathbf{u}^*_1 + f^* \hat{\mathbf{e}}_3 \times \mathbf{u}^*_1 = -g\nabla^*\eta^* \tag{3.1}$$

$$(\eta^* - h^*)_{t^*} + \nabla^* \cdot [\mathbf{u}^*_1(H + \eta^* - h^* - h^*_B)] = 0 \tag{3.2}$$

$$\mathbf{u}^*_{2t^*} + \mathbf{u}^*_2 \cdot \nabla^* \mathbf{u}^*_2 + f^* \hat{\mathbf{e}}_3 \times \mathbf{u}^*_2 = -\frac{1}{\rho_2}\nabla^* p^* - r^* \mathbf{u}^*_2 \tag{3.3}$$

$$h^*_{t^*} + \nabla^* \cdot (\mathbf{u}^*_2 h^*) = 0, \tag{3.4}$$

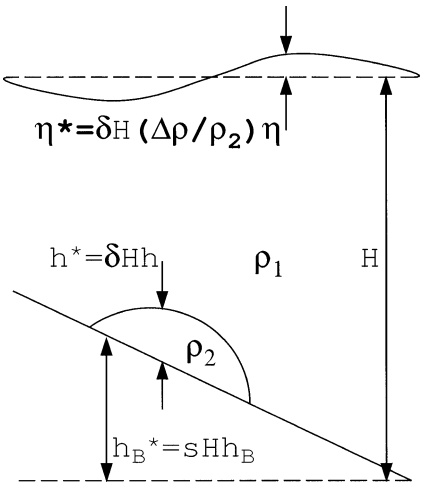

FIG. 1. The geometry of the problem and the interpretation of some of the nondimensional scalings. Asterisks denote dimensional variables. The model is derived assuming $\delta \ll 1$ and $s \ll 1$. The bottom topography is not necessarily linear.

where an asterisk denotes a dimensional variable. The upper and lower layer velocities are denoted by $\mathbf{u}_1$ and $\mathbf{u}_2$ respectively. H is the scale depth of the upper layer, h is the lower-layer thickness, h_B is the height of the bottom topography above an arbitrary reference level, η is the upper layer pressure, and the lower layer pressure p^* is given by

$$p^* = \rho_1 g\eta^* + \rho_2 g'(h^* + h^*_B), \tag{3.5}$$

where $g' = g(\rho_2 - \rho_1)/\rho_2$ is the reduced gravity. The form of the upper and lower layer pressure terms is such that the pressure vanishes at the upper-layer surface and the pressure is continuous across the interface between the two layers. Here, by ''pressure,'' we are referring to the dynamic pressure, where the hydrostatic component has been subtracted out. In the lower-layer momentum equation, we have retained the Rayleigh damping term, which parameterizes the effects of bottom friction.

The following generic scalings are used:

$$(x^*, y^*) = L(x, y), \qquad \mathbf{u}^*_1 = U_1\mathbf{u}_1, \qquad \mathbf{u}^*_2 = U_2\mathbf{u}_2,$$
$$t^* = Tt, \qquad f^* = f_0 f, \qquad r^* = f_0 r,$$
$$p^* = s\rho_2 g' H p, \qquad \eta^* = \frac{g'}{g}\delta H\eta, \qquad h^* = \delta H h,$$
$$h^*_B = sHh_B, \tag{3.6}$$

where $s = h^*_B/H = s^*L/H$ and $\delta = h^*/H$ are dimensionless parameters and s^* is the slope of the bottom topography. The parameters s and δ are the ratios of the scale height of, respectively, the bottom topography and the lower-layer thickness, to the scale height of the upper layer (see Fig. 1). A relatively thin lower layer and a gently sloping bottom correspond to $0 < \delta \ll 1$ and $0 < s \ll 1$.

Substituting the above scalings into the shallow-water equations yields

$$U_1\left(\frac{L}{T}\mathbf{u}_{1t} + U_1\mathbf{u}_1\cdot\boldsymbol{\nabla}\mathbf{u}_1\right) + f_0U_1Lf\hat{\mathbf{e}}_3\times\mathbf{u}_1 = -\delta g'H\boldsymbol{\nabla}\eta, \tag{3.7}$$

$$\boldsymbol{\nabla}\cdot\mathbf{u}_1 = sh_t + \boldsymbol{\nabla}\cdot[\mathbf{u}_1(\delta h + sh_B)], \tag{3.8}$$

$$U_2^2(\mathbf{u}_{2t} + \mathbf{u}_2\cdot\boldsymbol{\nabla}\mathbf{u}_2) + f_0U_2Lf\hat{\mathbf{e}}_3\times\mathbf{u}_2 = -g'H\boldsymbol{\nabla}[\delta(\eta + h) + sh_B] - f_0U_2Lr\mathbf{u}_2, \tag{3.9}$$

$$h_t + \boldsymbol{\nabla}\cdot(\mathbf{u}_2h) = 0. \tag{3.10}$$

Time has been scaled advectively with respect to the lower-layer velocity so that $T = L/U_2$. The rigid-lid approximation, which is valid for $g'/g \ll 1$, has been made by neglecting the η terms in the upper-layer conservation of mass equation (3.2) and the term proportional to g'/g in the lower-layer pressure continuity equation (3.5). The lower-layer height h and bottom topography h_B have been assumed to be much smaller in amplitude than the overlying ocean, and the upper and lower layer pressures have been scaled such that the upper-layer pressure strongly interacts with the lower-layer height. We have retained a generic dependence of the Coriolis parameter on latitude, $f = f(y)$.

b. Midlatitude scales

The nondimensional scalings of Swaters and Flierl (1991) are applicable at midlatitudes in the sense that employing their nondimensionalization leads to the description of geostrophically balanced flow. Therefore, in order to derive a model capable of describing geostrophically balanced flow (before that balance breaks down in the vicinity of the equator), the Swaters and Flierl (1991) scalings are employed here. Even though they may be applied within a few degrees latitude of the equator, we will refer to these scalings as the *midlatitude scalings* to distinguish them from a set of scalings, discussed later, that are applicable only in a near-equatorial region. The midlatitude scalings arise out of the generic scalings by setting

$$L = \frac{\sqrt{g'H}}{f_0}, \qquad U_1 = \delta f_0 L, \qquad T = \frac{1}{sf_0},$$

$$U_2 = \frac{g's^*}{f_0} = \frac{g'sH}{f_0L} = sf_0L = \frac{U_1}{\mu}, \tag{3.11}$$

where

$$\mu = \frac{\delta}{s}. \tag{3.12}$$

The parameter μ is one of the key parameters related to the stability characteristics of the Swaters and Flierl (1991) model, and we will refer to it as the interaction parameter. It is a measure of the ratio of the destabilizing effect of baroclinicity to the stabilizing effect of bottom slope (Swaters 1991, 1993).

The length scale is then the internal Rossby deformation radius of the upper layer, and the lower-layer velocity scale is the N83 along-slope speed. The parameter s is related to the slope of the bottom topography, s^*, via $s = s^*L/H$, and so is referred to as the scaled slope parameter. In these scalings, s also plays the role of the Rossby number of the flow,[1] by virtue of the definition for U_2,

$$s = \frac{U_2}{f_0L}.$$

We will, in general, assume that $s \ll 1$ so that s will serve as the small parameter in our asymptotic expansions.

This is consistent with observational data. Hall et al. (1997), using current meter moorings in the equatorial channel at 36°W, measured the time-mean velocity of AABW over 604 days to be approximately 5 cm s^{-1} with daily values over 10 cm s^{-1}, while McCartney and Curry (1993) measured the AABW velocity in the same location to be between 7 and 8 cm s^{-1} using the equatorial geostrophic relation. Sandoval and Weatherly (2001), in their synthesis of hydrographic data, suggest that the branch of AABW that crosses the equator flows at approximately 8 cm s^{-1}. That branch has a width of about 100 km at 4°30′S. These scales give $s = U_2/(f_0L) \approx 0.07$. Alternately, with a bottom slope of $s^* = 300$ m/100 km and with the depth of the overlying fluid taken as $H = 4.5$ km, $s = s^*L/H \approx 0.067$.

With the scalings (3.11), the governing equations now take the form

$$s(\mathbf{u}_{1t} + \mu\mathbf{u}_1\cdot\boldsymbol{\nabla}\mathbf{u}_1) + f\hat{\mathbf{e}}_3\times\mathbf{u}_1 = -\boldsymbol{\nabla}\eta, \tag{3.13}$$

$$\boldsymbol{\nabla}\cdot\mathbf{u}_1 = s\{h_t + \boldsymbol{\nabla}\cdot[\mathbf{u}_1(\mu h + h_B)]\}, \tag{3.14}$$

$$s(\mathbf{u}_{2t} + \mathbf{u}_2\cdot\boldsymbol{\nabla}\mathbf{u}_2) + f\hat{\mathbf{e}}_3\times\mathbf{u}_2 = -\boldsymbol{\nabla}[\mu(\eta + h) + h_B] - r\mathbf{u}_2, \tag{3.15}$$

$$h_t + \boldsymbol{\nabla}\cdot(\mathbf{u}_2h) = 0. \tag{3.16}$$

When $f \equiv 1$, the model is geostrophic to leading order, and expanding the dependent variables in terms of the asymptotic parameter s, as well as taking $r \to 0$, yields the Swaters and Flierl (1991) model.

The simplified model that we will obtain with these scalings is derived by forming the vorticity equation and the divergence equation of the upper layer. The divergence equation, which is formed by taking the divergence of the momentum equations, will provide a generalization of geostrophic balance that is valid at the equator. The upper-layer equations will be expressed in terms of a streamfunction and a velocity potential, using

[1] Here s is the temporal and advective Rossby number of the lower layer, but only the temporal Rossby number of the upper layer; δ is the advective Rossby number of the upper layer.

the theorem that the upper-layer velocity may be written as the sum of a nondivergent part and an irrotational part, that is, employing the Helmholtz decomposition

$$\mathbf{u}_1 = \hat{\mathbf{e}}_3 \times \nabla\psi + s\nabla\chi. \tag{3.17}$$

The irrotational part is assumed to be $O(s)$ because the divergence of the upper-layer velocity is $O(s)$ [see (3.14)].

The equations of motion written in terms of the vorticity and divergence equations of the upper layer and expressed in terms of ψ and χ are

$$s\Delta\psi_t + J(\psi, f + s\mu\Delta\psi) + s\nabla\chi\cdot\nabla(f + s\mu\Delta\psi) + s(f + s\mu\Delta\psi)[h_t + J(\psi, \mu h + h_B) + s(\mu h + h_B)\Delta\chi + s\nabla\chi\cdot\nabla(\mu h + h_B)] = 0, \tag{3.18}$$

$$s^2\Delta\chi_t + 2s\mu J(\psi_y, \psi_x) + s^2\mu[J(\psi, \Delta\chi) + 2J(\psi_x, \chi_x) + 2J(\psi_y, \chi_y)] + s^3\mu[\nabla\cdot(\Delta\chi\nabla\chi) + 2J(\chi_y, \chi_x)] - \nabla\cdot(f\nabla\psi) + sJ(\chi, f) + \Delta\eta = 0, \tag{3.19}$$

$$\Delta\chi = h_t + J(\psi, \mu h + h_B) + s\nabla\cdot[\nabla\chi(\mu h + h_B)], \tag{3.20}$$

$$s(\mathbf{u}_{2t} + \mathbf{u}_2\cdot\nabla\mathbf{u}_2) + f\hat{\mathbf{e}}_3\times\mathbf{u}_2 = -\nabla[\mu(\eta + h) + h_B] - r\mathbf{u}_2, \quad \text{and} \tag{3.21}$$

$$h_t + \nabla\cdot(\mathbf{u}_2 h) = 0, \tag{3.22}$$

where $J(A, B) = A_xB_y - A_yB_x$ is the Jacobian operator and $\Delta\psi = \hat{\mathbf{e}}_3\cdot\nabla\times\mathbf{u}_1$ is the relative vorticity of the upper layer by virtue of (3.17). The upper-layer conservation of mass (3.14) has been used to eliminate the divergence term from the upper-layer vorticity equation. This set of equations is, in fact, the full set of shallow-water equations stated in terms of ψ, χ, and s, and are valid for any s. This fact will be exploited when we derive a model valid for both midlatitude scalings and equatorial scalings simultaneously.

The model is derived in the $s \to 0$ asymptotic limit. While it may appear that the leading order part of the vorticity equation (3.18) is $J(\psi, f) = 0$, this is not true since, on the scales of motion we are considering, $df/dy = O(s)$ (and, of course, $df/dx = 0$). The alternate assumption, that df/dy does not scale with s, corresponds to considering basin-sized scales of motion. Our analysis does not apply to that scale since we have neglected other dynamics important on that scale such as wind-driven circulation, which induces vertical velocities. In fact, the leading-order vorticity balance on that scale is known to be $\beta v = f\partial w/\partial z$, where w is the vertical velocity, that is, the Sverdrup relation (Pedlosky 1996). Note that $J(\psi, f) = 0$ is the Sverdrup relation with $w \equiv 0$.

c. Equatorial Model I

In the limit as $s \to 0$, the leading-order model derived from a midlatitude scaling is

$$\Delta\psi_t + J(\psi, f/s + \mu\Delta\psi) + f[h_t + J(\psi, \mu h + h_B)] = 0, \tag{3.23}$$

$$\Delta\eta = \nabla\cdot(f\nabla\psi), \tag{3.24}$$

$$h_t + \nabla\cdot(\mathbf{u}_2 h) = 0, \tag{3.25}$$

$$s(\mathbf{u}_{2t} + \mathbf{u}_2\cdot\nabla\mathbf{u}_2) + f\hat{\mathbf{e}}_3\times\mathbf{u}_2 = -\nabla[\mu(\eta + h) + h_B] - r\mathbf{u}_2. \tag{3.26}$$

Note that the $\nabla\chi\cdot\nabla f$ term has been neglected since $df/dy = O(s)$. This removes χ from the leading-order problem.

The leading-order divergence equation (3.24) is a generalization of geostrophic balance. When $f \equiv 1$ (and with identical boundary conditions on η and ψ), this reduces to $\eta = \psi$ (to within a harmonic function), the statement that the geostrophic pressure is the streamfunction for the flow. Equation (3.24) is the divergence equation in the ''linear balance equations'' of Gent and McWilliams (1983). Additionally, note that this relation contains within it the equatorial geostrophic relation $\beta u = -\eta_{yy}$, where β is the meridional derivative of the Coriolis parameter. The equatorial geostrophic relation may be derived by taking the meridional derivative of the expression of geostrophic balance between the zonal velocity and the meridional pressure gradient, assuming that the meridional pressure gradient vanishes right on the equator (Jerlov 1953). At $f = 0$, (3.24) reduces to $\Delta\eta = \beta\psi_y$, which simplifies to the equatorial geostrophic relation if it is further assumed that $\eta_{xx} = 0$.

Although the model was derived from a midlatitude scaling, it allows f to vary and, indeed, no singularities arise in the $f \to 0$ limit. It is straightforward to check that, as $f \to 1$ and $r \to 0$, this system reduces to the Swaters and Flierl (1991) model. Thus, (3.23)–(3.26) is a generalization of their model that describes well-defined flow at the equator. We will refer to this model as the Equatorial Model I, henceforth abbreviated as the EMI model.

In the lower-layer momentum equation (3.26), we have retained both the $O(s)$ inertial terms and the $O(r)$ frictional term. In the $s \ll r$ limit, the frictional geo-

strophic model discussed by CS02 is recovered. In the $r \ll s$ limit, the frictionless and inertial shallow-water model, with s as a Rossby number, is recovered. Thus, the model as written is general enough to employ either of the one-layer models studied by CS02 to govern the lower-layer dynamics.

d. EMI model simulations

Numerical simulations of this model will allow us to assess whether this model does, in fact, reproduce the behavior of the Swaters and Flierl (1991) and to investigate near-equatorial behavior.

The numerical procedure used is similar to the procedure of Swaters (1998) for the upper-layer equations, and identical to the procedure described in CS02 for the lower-layer equations. At each time step, we solve the model equations in the following order:

$$
\begin{aligned}
&q_t + J(\psi, q + f - fh) + fJ(\psi, h + h_B) = 0,\\
&s(\mathbf{u}_{2t} + \mathbf{u}_2 \cdot \boldsymbol{\nabla}\mathbf{u}_2) + f\hat{\mathbf{e}}_3 \times \mathbf{u}_2\\
&\quad = -\boldsymbol{\nabla}[\mu(\eta + h) + h_B] - r\mathbf{u}_2,\\
&h_t + \boldsymbol{\nabla} \cdot (\mathbf{u}_2 h) = 0,\\
&\Delta\psi = q - fh,\\
&\Delta\eta = \frac{df}{dy}\psi_y + f(q - fh),
\end{aligned}
$$

where the vorticity $q = \Delta\psi + fh$ is updated using a leapfrog time discretization, Arakawa and Lamb (1981) schemes are employed for the Jacobian terms, and the Laplacian operators are inverted using a direct solver (Swaters 1998). The spatial discretization of the lower-layer momentum equation is performed using the Arakawa and Hsu (1990) scheme, and the time stepping is done using the third-order scheme of Matsuno (1966). The lower-layer height field is advanced via methods described in Hsu and Arakawa (1990).

We begin with a test simulation of the EMI model where $f = 1$, $r = 0$, and the bottom topography is that of a linearly sloping shelf, $h_B = -y$. Under the conditions of $f = 1$ and $r = 0$, the model should reduce to the Swaters (1991) model.

The simulation shown in Fig. 2 should be compared with Plate 1 of Swaters (1998). The baroclinic instabilities characteristic of the Swaters and Flierl (1991) model that are preferentially amplified on the downslope side of the current are clearly seen. Throughout the simulation, the η and ψ functions are identical. This confirms that the EMI model derived is, indeed, a generalization of the Swaters and Flierl (1991) model to the case of varying Coriolis parameter, including allowing for $f = 0$ in the domain.

Choboter and Swaters (2000) investigated the dynamics of equator-crossing currents using simplified one-layer models and idealized topography. To explore the effects of baroclinicity on near-equatorial motions in the EMI model, we reproduce the simulations of Choboter and Swaters (2000), with and without a dynamically active upper layer, and quantitatively compare the results (Figs. 3–7).

Choboter and Swaters (2000) compared the dynamics of a ''frictional geostrophic'' (henceforth FG) model with the dynamics of the shallow-water equations. The FG model may be written

$$
u = g'\frac{-fp_y - rp_x}{f^2 + r^2}, \qquad v = g'\frac{fp_x - rp_y}{f^2 + r^2},
$$

$$
h_t + \boldsymbol{\nabla} \cdot (\mathbf{u}h) = 0,
$$

where $p = h + h_B$. This model is simply the balance between the Coriolis effect and frictional drag that results from setting $s = 0$ and $\eta = 0$ in the lower-layer equations, (3.25) and (3.26), of the EMI model. They compared the two models by simulating the evolution of an eddy approaching the equator from the south along the western flank of a north–south channel. This was done to observe the breakdown of geostrophic balance in the fluid as it approached the equator, and for comparison with the similar shallow-water simulations of Borisov and Nof (1998). The channel used by Choboter and Swaters (2000) was specified to be $h_B = \sqrt{x^2 + 1}$, and the latitudinal variation of the Coriolis parameter was $f = \tanh(y)$. The same functional form of the topography and Coriolis parameter are used here.

The use of $f = f_0 \tanh(\beta L y/f_0)$ as the Coriolis parameter allows f-plane dynamics to be recovered when $|y| \gg f_0/\beta L$ and equatorial β-plane dynamics to be recovered when $|y| \ll f_0/\beta L$. One goal of the present work is to investigate models of abyssal flows valid in both regimes, and the use of such form of f, while unrealistic, does allow for the observation of the transition of the flow from f-plane dynamics, through β-plane dynamics, and back to f-plane dynamics after passing through the equator. The application of simplified models using realistic Coriolis parameter and topography is the focus of CS02.

In simulations of a northward-propagating eddy along the western slope of the channel, both FG dynamics (Fig. 3) and shallow-water dynamics (Fig. 4) predict that the lens flows northward along the slope, then turns eastward along the equator, and finally splits into northward- and southward-flowing parts along the eastern slope. This motion is very similar to the one-layer shallow-water simulations of Borisov and Nof (1998) and is consistent with the observations of Johnson et al. (1991), who find that the northward-flowing deep western boundary current in the Somali Basin turns eastward at the equator.

Notable differences between the shallow-water simulation and the FG simulation include the fact that the shallow-water lens penetrates the equator as it turns eastward where the FG eddy does not and that fluid in the shallow-water simulation flows to a higher point on the eastern slope than fluid in the FG simulation. These

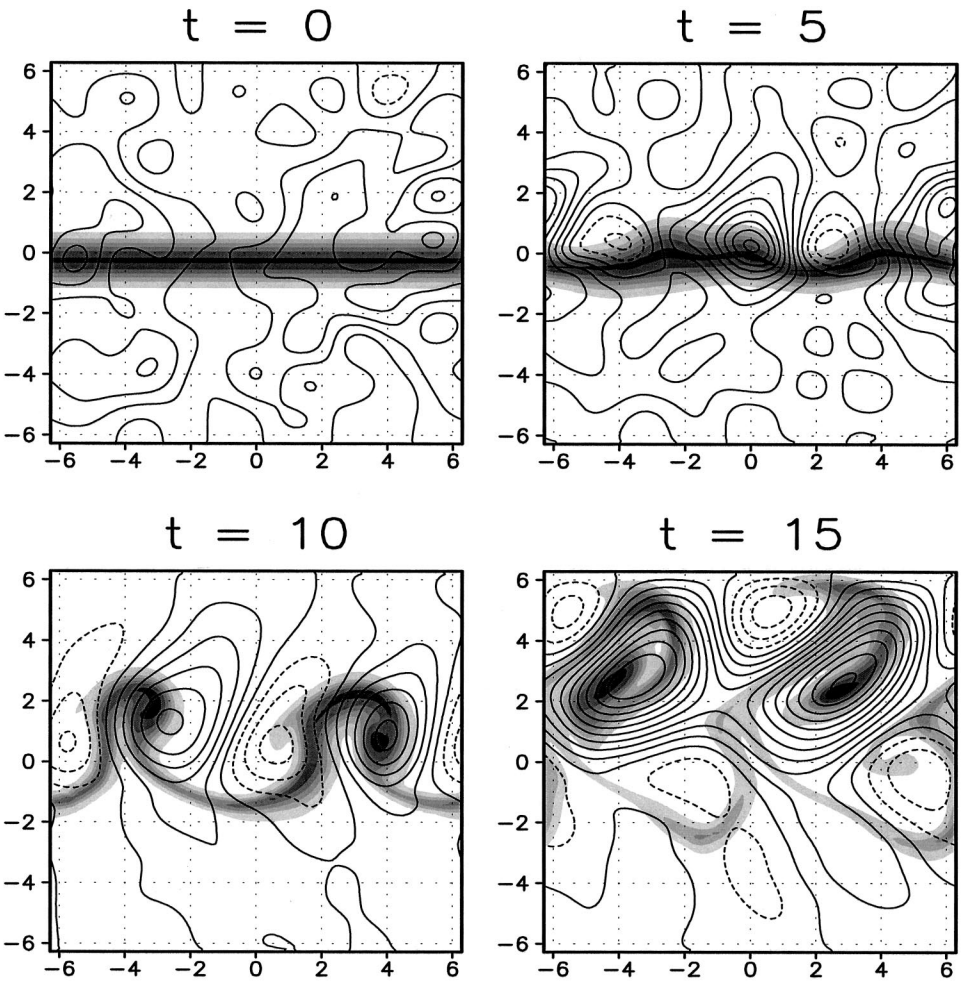

FIG. 2. EMI simulation with $f = 1$, $r = 0$, and $h_B = -y$. The shaded region is the lower-layer height; darker corresponds to higher values. Contours are of the upper-layer pressure η. The streamfunction ψ is exactly equal to η. Contour interval is 0.05 for $t = 0$ and 5 and 0.25 for $t = 10$ and 15. Dotted contours denote negative values.

two differences hold over the whole range of parameters tested, and both are a result of the lack of fluid inertia in the FG model (Choboter and Swaters 2000).

For each of the numerical experiments where it is appropriate to compare with the single-layer simulations of Choboter and Swaters (2000), the model is simulated once with an active upper layer and once without an active upper layer, with all other conditions the same. The effect of the upper layer is measured by the point-by-point difference in the lower-layer height between the two simulations, and displayed as contours of

$$h_{\text{diff}} = h_{\text{1-layer}} - h_{\text{2-layer}},$$

where $h_{\text{1-layer}}$ is the height with no upper layer present and $h_{\text{2-layer}}$ is the height in the presence of an active upper layer. This difference is typically small as compared to the height itself.

In the simulations of the EMI model over idealized meridional channel topography (Figs. 3, 4, and 7), little qualitative difference is seen between the one- and two-layer model simulations. The difference that does exist implies that the lens in the two-layer simulation is slightly lower on the slope than in the one-layer simulation, suggesting that the two-layer eddy has given up some of its potential energy to spin up the upper layer.

Whether the lower layer is governed by FG dynamics (Fig. 3) or by shallow-water dynamics (Fig. 4), there does not appear to be much wave motion in the upper layer. We have not been able to identify waves in the EMI model that propagate along the equatorial waveguide, neither analytically nor in numerical experiments (Fig. 5).

The meridional-channel experiments displayed thus far have all been performed with Dirichlet boundary conditions. Runs were also performed with periodic conditions in the zonal direction, to ensure the bound-

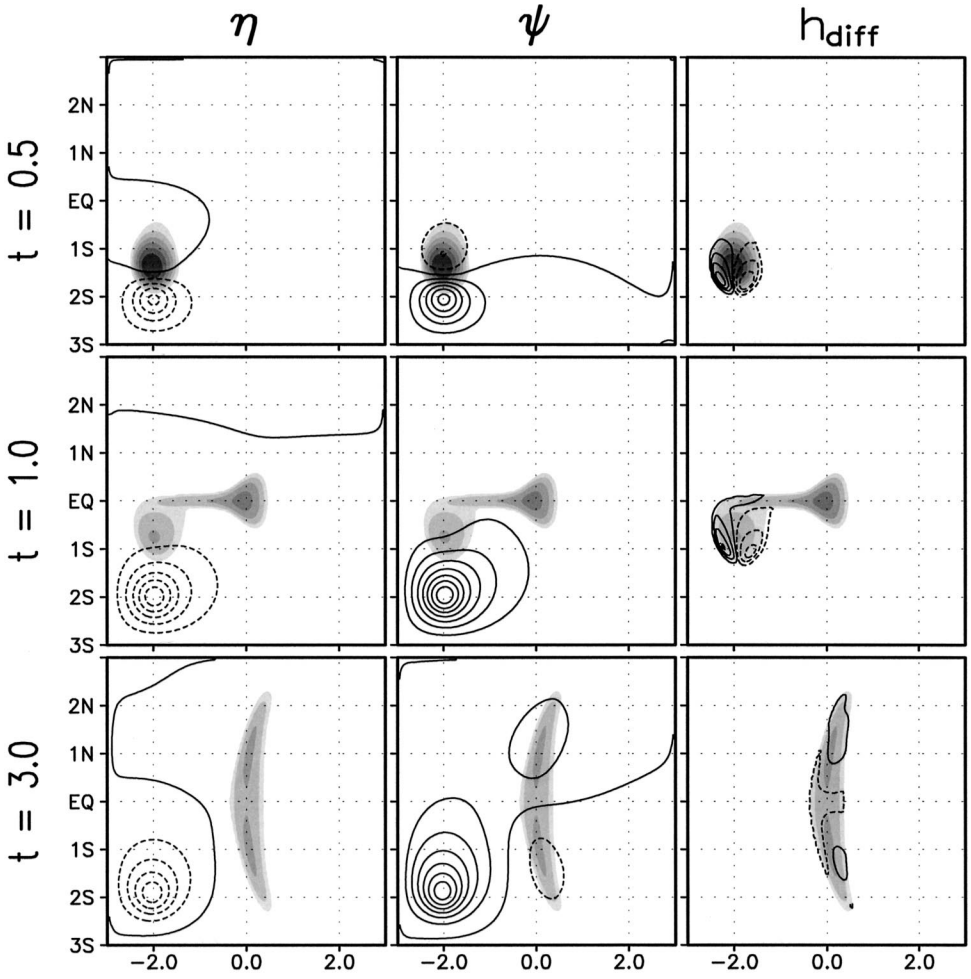

FIG. 3. EMI simulation where lower layer is governed by FG model; $f = \tanh(y)$ and $h_B = \sqrt{x^2 + 1}$. The shaded region is the lower-layer height; darker corresponds to higher values. Contours are of the upper layer pressure η, streamfunction ψ, or h_{diff}, where $h_{\text{diff}} = h_{\text{1-layer}} - h_{\text{2-layer}}$. Contour interval is 0.005, with ± 0.001 replacing the zero contour for h_{diff}. The y-axis labels do not represent degrees of latitude but rather nondimensional length units north or south of $f = 0$.

aries were not impeding wave motions in the upper layer (Fig. 6). The upper-layer eddy, which was spun up from the initial conditions, remains stationary. There is a slow drift, but it is on much slower timescales than the behavior of the lower layer.

There is nothing in the derivation of the model that restricts it to the description of domes of fluid in the lower layer: the model is general enough to simulate lower-layer currents as well. EMI model simulations with and without an upper layer have been performed with a local flux of lower-layer fluid into the domain to simulate the northward flow of a current instead of an isolated eddy (Fig. 7). Qualitatively, these simulations compare well with the one-layer shallow-water simulations of Nof and Borisov (1998). The path of the current is similar to that of shallow-water eddies. This is not surprising, given that, when a dome of fluid impacts the equator, it resembles a current as it flows downhill along the equator.

We emphasize that exactly the same dynamical model is responsible for the dynamics of every one of the simulations displayed in Figs. 2–7. Yet, in Fig. 2, where $f \neq 0$ in the domain, the baroclinic coupling dominated the dynamics by driving the instability, while in the remaining experiments, where $f = 0$ in the domain, the coupling had a very weak effect on the dynamics. The same weakening of the coupling mechanism in the $f = 0$ limit may be seen analytically in the near-equatorial models of two-layer flow we derive in the next section.

4. Equatorial models II and III

The usual nondimensional scaling in the study of equatorial dynamics uses the equatorial deformation ra-

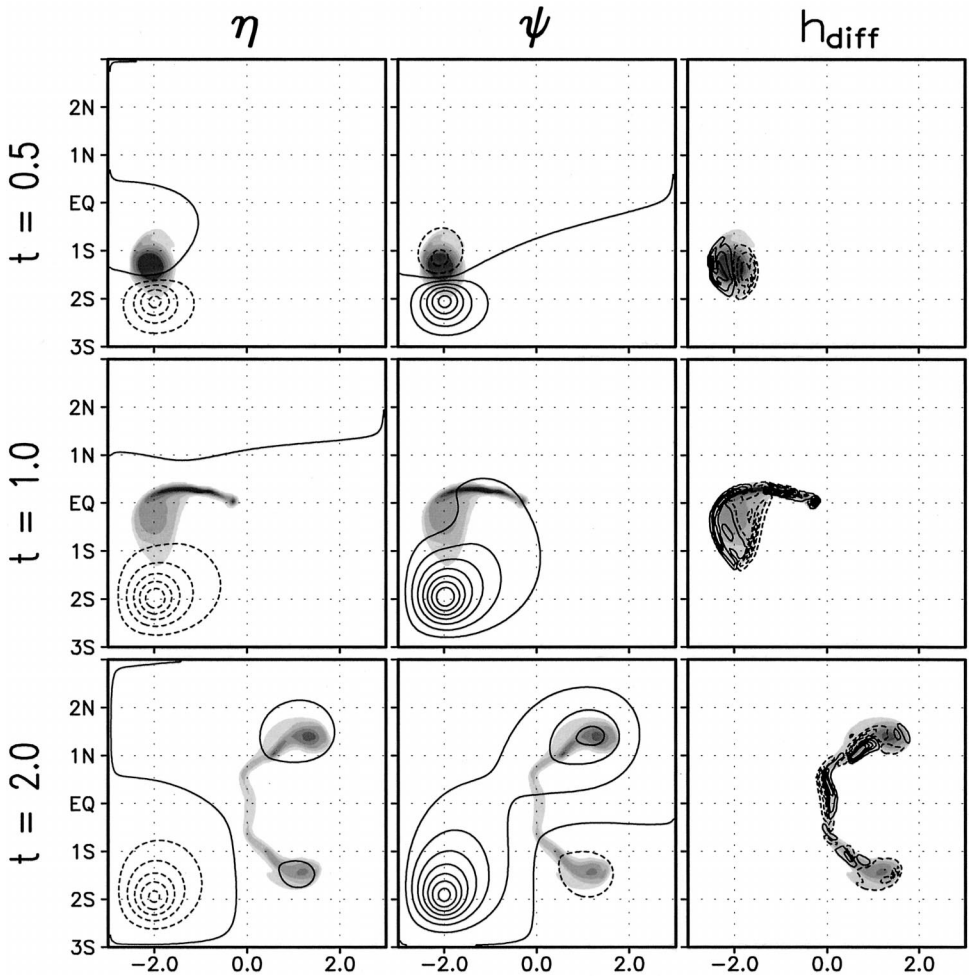

FIG. 4. EMI simulation where lower layer is governed by the shallow-water model; $f = \tanh(y)$ and $h_B = \sqrt{x^2 + 1}$. The shaded region is the lower-layer height; darker corresponds to higher values. Contours are of the upper-layer pressure η, streamfunction ψ, or h_{diff}, where $h_{\text{diff}} = h_{\text{1-layer}} - h_{\text{2-layer}}$. Contour interval is 0.005, with ± 0.001 replacing the zero contour for h_{diff}.

dius as the length scale (Cushman-Roisin 1994). The equatorial scaling may be conveniently stated by replacing f_0 in the midlatitude scaling (3.11) with $\beta_0 L$, where $\beta_0 = df/dy$ at $y = 0$:

$$L = \frac{\sqrt{g'sH}}{\beta_0 L}, \qquad U_1 = \mu\beta_0 L^2, \qquad T = \frac{1}{\beta_0 L},$$

$$U_2 = \frac{g's^*}{\beta_0 L} = \frac{g'sH}{\beta_0 L^2} = \beta_0 L^2 = U_1/\mu, \tag{4.1}$$

Note that the N83 velocity scaling is retained, but the length scale is now the internal Rossby deformation radius of the *lower* layer. We have scaled the velocity slightly differently in the two layers, incorporating the interaction parameter μ (Swaters 1991) in the same way as in the midlatitude scaling. With the scaling (4.1), the equations of motion (3.7)–(3.10) become

$$\mathbf{u}_{1t} + \mu\mathbf{u}_1 \cdot \nabla\mathbf{u}_1 + f\hat{\mathbf{e}}_3 \times \mathbf{u}_1 = -\nabla\eta, \tag{4.2}$$

$$\nabla \cdot \mathbf{u}_1 = s\{h_t + \nabla \cdot [\mathbf{u}_1(\mu h + h_B)]\}, \tag{4.3}$$

$$\mathbf{u}_{2t} + \mathbf{u}_2 \cdot \nabla\mathbf{u}_2 + f\hat{\mathbf{e}}_3 \times \mathbf{u}_2 = -\nabla[\mu(\eta + h) + h_B] - r\mathbf{u}_2, \tag{4.4}$$

$$h_t + \nabla \cdot (\mathbf{u}_2 h) = 0. \tag{4.5}$$

The momentum equations scaled for equatorial flow do not undergo great simplification upon imposing the $s \ll 1$ assumption. However, in the upper layer, the conservation of mass equation implies that one may employ the Helmholtz decomposition (3.17), where the irrotational part is $O(s)$. The derivation of the leading-order model is similar to the derivation of EMI, so the intermediate steps are omitted for brevity. By forming the vorticity and divergence equations, writing the upper-layer equations in terms of ψ and χ, and neglecting the

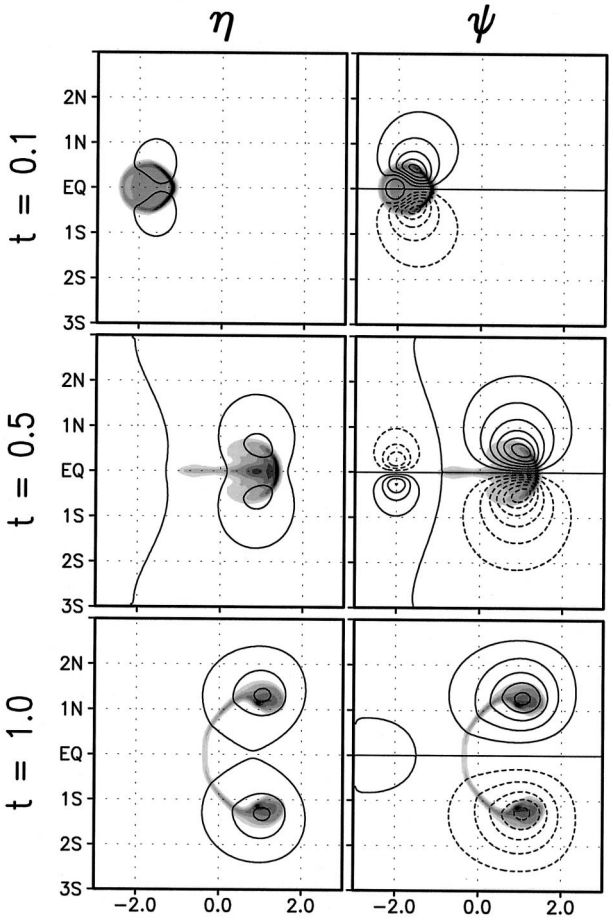

FIG. 5. EMI simulation, eastward eddy with shallow-water dynamics in the lower layer; $f = \tanh(y)$ and $h_B = \sqrt{x^2 + 1}$. The shaded region is the lower-layer height; darker corresponds to higher values. Contours are of the upper-layer pressure η or streamfunction ψ. Contour interval is 0.00025 for $t = 0.1$ and 0.5 and 0.0025 for $t = 1.0$.

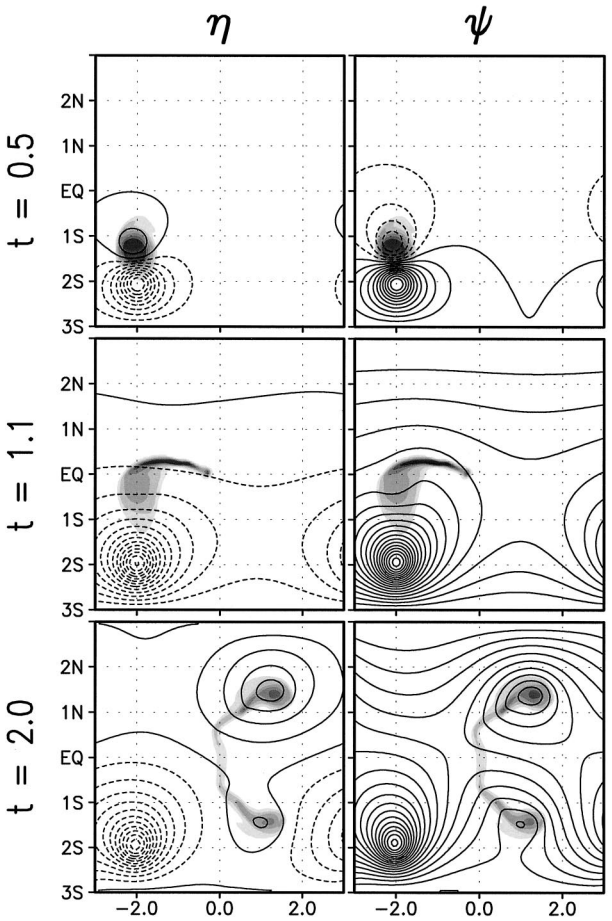

FIG. 6. EMI simulation where lower layer is governed by the shallow-water model, periodic conditions; $f = \tanh(y)$ and $h_B = \sqrt{x^2 + 1}$. The shaded region is the lower-layer height; darker corresponds to higher values. Contours are of the upper-layer pressure η or streamfunction ψ. Contour interval is 0.0025.

$O(s)$ terms, Equatorial Model II (EMII) may be derived in the form:

$$\Delta\psi_t + J(\psi, f + \mu\Delta\psi) = 0, \tag{4.6}$$

$$\Delta\eta = \nabla \cdot (f\nabla\psi) + 2\mu J(\psi_x, \psi_y), \tag{4.7}$$

$$\mathbf{u}_{2t} + \mathbf{u}_2 \cdot \nabla\mathbf{u}_2 + f\hat{\mathbf{e}}_3 \times \mathbf{u}_2 = -\nabla[\mu(\eta + h) + h_B], \tag{4.8}$$

$$h_t + \nabla \cdot (\mathbf{u}_2 h) = 0. \tag{4.9}$$

Note that, in the equatorial scaling, $df/dy = O(1)$, so the $J(\psi, f)$ term is retained.

The upper-layer variables are not at all affected by the lower-layer variables. The model remains partially coupled in the sense that motions in the upper layer will influence the lower-layer variables. However, there is nothing to induce motions in the upper-layer streamfunction except perhaps boundary forcing; that is, streamfunction may be forced by waves propagating in from the far field. If the upper-layer streamfunction is not driven by boundary forcing, then the solution to (4.6) is $\psi = 0$. This is consistent with the previous scaling assumptions if ψ is, in fact, an $O(s)$ quantity. Explicitly rescaling ψ in this way leads to a third equatorial model.

In order to derive a model where the streamfunction is an $O(s)$ quantity to leading order, ψ is rescaled so that

$$\psi = s\tilde{\psi},$$

where $\tilde{\psi} = O(1)$. For a self-consistent model, η must be rescaled in the same way:

$$\eta = s\tilde{\eta}, \qquad \tilde{\eta} = O(1).$$

With these assumptions, following a derivation similar to that of the first two models yields Equatorial Model III (EMIII):

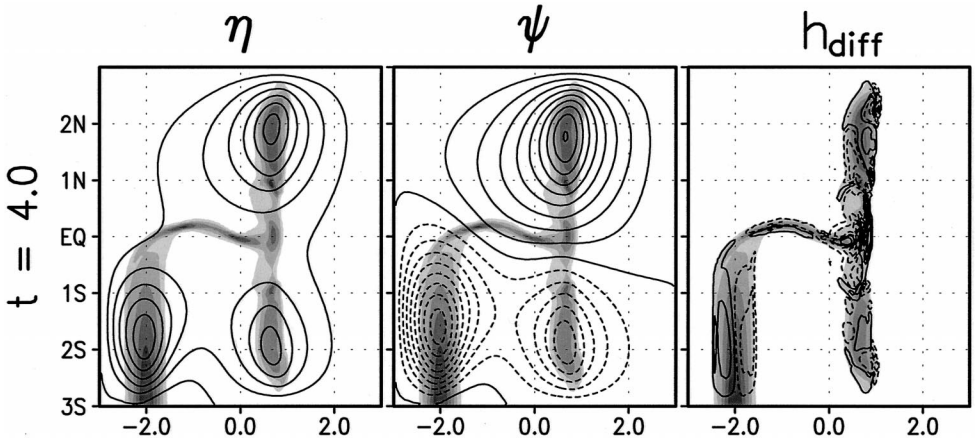

FIG. 7. EMI simulation of an inflow current; lower layer is governed by the shallow-water model; $f = \tanh(y)$ and $h_B = \sqrt{x^2 + 1}$. The shaded region is the lower-layer height; darker corresponds to higher values. Contours are of the upper-layer pressure η, streamfunction ψ, or h_{diff}, where $h_{\text{diff}} = h_{\text{1-layer}} - h_{\text{2-layer}}$. Contour interval is 0.0025 for η and ψ and 0.005 for h_{diff}.

$$\Delta\tilde{\psi}_t + J(\tilde{\psi}, f) + \nabla\chi\cdot\nabla f + fh_t = 0, \tag{4.10}$$

$$\Delta\chi_t + \Delta\tilde{\eta} = \nabla\cdot(f\nabla\tilde{\psi}) + J(f, \chi), \tag{4.11}$$

$$\Delta\chi = h_t, \tag{4.12}$$

$$\mathbf{u}_{2t} + \mathbf{u}_2\cdot\nabla\mathbf{u}_2 + f\hat{\mathbf{e}}_3\times\mathbf{u}_2 = -\nabla(\mu h + h_B), \tag{4.13}$$

$$h_t + \nabla\cdot(\mathbf{u}_2 h) = 0. \tag{4.14}$$

The velocity potential χ is retained at leading order in the divergence equation (4.11), so an extra equation has been added to close the system. That equation is (4.12), which comes from the upper-layer conservation of mass (4.3).

Note that the equations governing the upper layer, (4.10)–(4.12), may be derived without approximation from the set of equations:

$$u_t - fv = -\tilde{\eta}_x, \qquad v_t + fu = -\tilde{\eta}_y,$$
$$h_t = u_x + v_y, \qquad u = \chi_x - \tilde{\psi}_y,$$
$$v = \chi_y + \tilde{\psi}_x,$$

which are exactly the linearized shallow-water or long-wave equations under the rigid-lid assumption. Thus the dynamics of this model are that of two-layer shallow-water dynamics under the rigid-lid assumption and with linearized upper-layer dynamics. The upper-layer variables are removed from the lower-layer dynamics to leading order. The motion in the lower layer is still forced by the sloping topography, so the solution of the lower layer is not that of no motion.

Each of the two models derived from equatorial scales of motion is a partially uncoupled model. In the EMII model (4.6)–(4.9), the upper-layer variables are not directly affected by the lower-layer variables, and in the EMII model (4.10)–(4.14), the lower-layer variables are not directly affected by the upper-layer variables. This weakening of the coupling mechanism in the vicinity of the equator lends support to the relevance of the reduced-gravity simulations studied by CS02.

5. Uniformly valid model

It is possible to identify in the midlatitude derivation of EMI those terms that emerge in the leading-order equatorial models of EMII and EMIII. By retaining those terms in the midlatitude model, we will find a model that is, to leading order, uniformly valid. We retain exactly those higher-order terms that, although not leading-order terms at midlatitudes, contribute to the leading-order balance in the equatorial limit.

The complete model, which we will refer to as the metamodel, may be written

$$\Delta\psi_t + J(\psi, f/s + \mu\Delta\psi) + \nabla\chi\cdot\nabla f + f[h_t + J(\psi, \mu h + h_B)] = 0, \tag{5.1}$$

$$\Delta\eta = \nabla\cdot(f\nabla\psi) + 2s\mu J(\psi_x, \psi_y) - s^2\Delta\chi_t + sJ(f, \chi), \tag{5.2}$$

$$\Delta\chi = h_t, \tag{5.3}$$

$$h_t + \nabla\cdot(\mathbf{u}_2 h) = 0, \tag{5.4}$$

$$s(\mathbf{u}_{2t} + \mathbf{u}_2\cdot\nabla\mathbf{u}_2) + f\hat{\mathbf{e}}_3\times\mathbf{u}_2 = -\nabla[\mu(\eta + h) + h_B] - r\mathbf{u}_2. \tag{5.5}$$

The form of the divergence equation (5.2) is consistent with the family of balance models studied by Gent and McWilliams (1983). The balance when $s \to 0$, which is the balance found in the midlatitude scaling model, is part of the linear balance equations (LBE). The balance retaining the leading-order plus the $J(\psi_x, \psi_y)$ term, which is the balance found in the equatorial scaling with boundary forcing, corresponds to the balance equations (BE). Retaining the leading-order terms plus the $J(f, \chi)$

TABLE 1. Length-, velocity-, and timescales in the midlatitude and equatorial nondemensional scalings. $R_d = \sqrt{g'H}/f_0$ is the internal Rossby deformation radius of the upper layer. Here $f_0 = \beta_0 L$ in the equatorial scaling.

Midlatitude	Equatorial
$L = R_d$	$L = s^{1/2} R_d$
$U_1 = \mu s f_0 R_d$	$U_1 = \mu s^{1/2} f_0 R_d$
$U_2 = s f_0 R_d$	$U_2 = s^{1/2} f_0 R_d$
$T = L/U_2$	$T = L/U_2$

term produces the balance equation of the global linear balance equations (GLBE), and retaining all the terms except $\Delta\chi_t$ yields the balance equation for the global balance equations (GBE).

Adjustment of length, velocity, and timescales

The metamodel as written is expressed in terms of variables that have been nondimensionalized using the midlatitude scaling. To show explicitly that this model contains the equatorial scaling models EMII and EMIII within its dynamics, we rescale the uniform model using the equatorial nondimensional scales. That is, we shall show that the metamodel, when expressed in equatorial variables, recovers the leading-order equatorial models, and therefore is a uniformly valid model.

To do this, it will be useful to find a simple relation between the equatorial and midlatitude sets of nondimensionalizing scales. When the length, time, and velocity scales are written in terms of the internal Rossby deformation radius of the upper layer,

$$R_d = \frac{\sqrt{g'H}}{f_0},$$

where f_0 stands for $\beta_0 L$ in the equatorial scalings, and the scales only differ by powers of s (see Table 1). Thus, denoting equatorial variables (nondimensional variables that have been scaled by the equatorial scalings) with a caret and the midlatitude variables without a caret:

$$(x, y) = s^{1/2}(\hat{x}, \hat{y}), \qquad t = s\hat{t},$$
$$\mathbf{u}_1 = s^{-1/2}\hat{\mathbf{u}}_1, \qquad \mathbf{u}_2 = s^{-1/2}\hat{\mathbf{u}}_2.$$

We must scale ψ and χ as well. The nondimensionalization of ψ and χ arises directly from their definition in the Helmholtz decomposition of u_1 (3.17),

$$\psi^* = LU_1\psi, \qquad \chi^* = sLU_1\chi.$$

Therefore, ψ and χ actually scale exactly the same in both coordinates,

$$\psi = \hat{\psi}, \qquad \chi = \hat{\chi}.$$

There is no need to express the variables h, h_B, η, and f in terms of equatorial variables since their scales are set in the generic nondimensionalization, independent of U_1, U_2, L, or T. Writing the metamodel equations (5.1)–(5.5) in terms of equatorial variables, they transform to

$$\hat{\Delta}\hat{\psi}_{\hat{t}} + \hat{J}(\hat{\psi}, f + \mu\hat{\Delta}\hat{\psi}) + s\hat{\boldsymbol{\nabla}}\hat{\chi}\cdot\hat{\boldsymbol{\nabla}}f + sf[h_{\hat{t}} + \hat{J}(\hat{\psi}, \mu h + h_B)] = 0, \tag{5.6}$$

$$\hat{\Delta}\eta = \hat{\boldsymbol{\nabla}}\cdot(f\hat{\boldsymbol{\nabla}}\hat{\psi}) + 2\mu\hat{J}(\hat{\psi}_{\hat{x}}, \hat{\psi}_{\hat{y}}) - s\hat{\Delta}\hat{\chi}_{\hat{t}} + s\hat{J}(f, \hat{\chi}), \tag{5.7}$$

$$\hat{\Delta}\hat{\chi} = h_{\hat{t}}, \tag{5.8}$$

$$h_{\hat{t}} + \hat{\boldsymbol{\nabla}}\cdot(\hat{\mathbf{u}}_2 h) = 0, \tag{5.9}$$

$$\hat{\mathbf{u}}_{2\hat{t}} + \hat{\mathbf{u}}_2\cdot\hat{\boldsymbol{\nabla}}\hat{\mathbf{u}}_2 + f\hat{\mathbf{e}}_3\times\hat{\mathbf{u}}_2 = -\hat{\boldsymbol{\nabla}}[\mu(\eta + h) + h_B] - r\hat{\mathbf{u}}_2. \tag{5.10}$$

At leading order, this reduces to the boundary-forced equatorial model EMII. Therefore, the metamodel contains within it the dynamics described by that model.

It remains to investigate whether or not the lower-layer-forced equatorial model (EMIII) is contained within the metamodel. In that model, the ψ and η fields are a factor of s smaller than in the boundary-forced equatorial model. That is,

$$\hat{\psi} = s\hat{\tilde{\psi}}, \qquad \eta = s\hat{\tilde{\eta}},$$

which, upon substituting into the set of equations (5.6)–(5.10), transforms them into the form

$$\hat{\Delta}\hat{\tilde{\psi}}_{\hat{t}} + \hat{J}(\hat{\tilde{\psi}}, f + s\mu\hat{\Delta}\hat{\tilde{\psi}}) + \hat{\boldsymbol{\nabla}}\hat{\chi}\cdot\hat{\boldsymbol{\nabla}}f + f[h_{\hat{t}} + s\hat{J}(\hat{\tilde{\psi}}, \mu h + h_B)] = 0, \tag{5.11}$$

$$\hat{\Delta}\hat{\tilde{\eta}} = \hat{\boldsymbol{\nabla}}\cdot(f\hat{\boldsymbol{\nabla}}\hat{\tilde{\psi}}) + 2s\mu\hat{J}(\hat{\tilde{\psi}}_{\hat{x}}, \hat{\tilde{\psi}}_{\hat{y}}) - \hat{\Delta}\hat{\chi}_{\hat{t}} + \hat{J}(f, \hat{\chi}), \tag{5.12}$$

$$\hat{\Delta}\hat{\chi} = h_{\hat{t}}, \tag{5.13}$$

$$h_{\hat{t}} + \hat{\boldsymbol{\nabla}}\cdot(\hat{\mathbf{u}}_2 h) = 0, \tag{5.14}$$

$$\hat{\mathbf{u}}_{2\hat{t}} + \hat{\mathbf{u}}_2\cdot\hat{\boldsymbol{\nabla}}\hat{\mathbf{u}}_2 + f\hat{\mathbf{e}}_3\times\hat{\mathbf{u}}_2 = -\hat{\boldsymbol{\nabla}}[s\mu(\eta + h) + h_B] - r\hat{\mathbf{u}}_2. \tag{5.15}$$

At leading order, this set of equations reduces to the EMIII model. This completes the proof that the metamodel is indeed a leading-order uniformly valid model.

We note that it remains for future research to investigate the uniformly valid model numerically. Since this model contains within it two-layer shallow-water dynamics (with linear upper-layer dynamics), it contains faster scales of motion than the slow dynamics of Swaters and Flierl (1991). Another difficulty is the fact that the $s^2\Delta\chi_t$ term in the divergence equation is multiplied by a small parameter, suggesting that the evolution of $\Delta\chi$ itself may be rapid.

6. Summary

We have investigated the influence of an upper layer of fluid on the dynamics of abyssal equator-crossing

eddies and currents. An analytical expression was derived for the steady propagation of an eddy on a slope under the f-plane approximation, where the effects of an upper layer and friction were taken into account. The presence of the upper layer was shown to reintroduce the possibility of upslope motion, where friction by itself had permitted only downslope motion.

Three new models of two-layer flow were derived. Equatorial Model I (EMI) is a direct extension of the Swaters and Flierl (1991) model to the case of varying Coriolis parameter f, including the case where $f = 0$ is in the domain of interest. The EMII model was shown to contain linear shallow-water dynamics in the upper layer and nonlinear shallow-water dynamics in the lower layer. Both EMII and EMIII are only partially coupled in their dynamics, and EMI appears uncoupled in the $f \rightarrow 0$ limit, based on the form of the model equations and on simple numerical tests. This supports the single-layer reduced-gravity simulations of CS02.

A leading-order uniformly valid metamodel was identified. This model was shown to be the simplest possible model that contains within it the three models already derived.

A striking feature of the models discussed here is that, while the midlatitude behavior is dominated by baroclinic interactions between the upper and lower layers, the equatorial dynamics display relatively little interaction. This implies that the nature of baroclinicity of abyssal flows at midlatitudes is fundamentally different than in the near-equatorial region. One may have been able to anticipate this from the large-scale potential vorticity point of view. Hallberg and Rhines (1996), in their investigation of two-layer shallow-water motion over topography, emphasize the importance of potential vorticity contours as lines along which flow in each layer is easily induced. The lack of motion in the upper layer of our equatorial simulations may be related to the fact that topographic potential vorticity contours are blocked at the equator.

One use of having a model valid at midlatitudes and at the equator is that one may exploit such a model to address questions relating the two regions. It remains for future research to address issues such as where the transition from midlatitude to equatorial dynamics occurs, comparing and contrasting midlatitude versus equatorial instabilities, and extending the model to the case of similar thicknesses between the two layers.

Acknowledgments. PFC gratefully acknowledges the funding received from the Natural Sciences and Engineering Research Council of Canada (NSERC) in the form of their PGS B scholarship, and from the Killam Foundation in the form of the Killam Memorial Ph.D. Scholarship. GES gratefully acknowledges continued support by NSERC in the form of ongoing Research Grants. Two anonymous reviewers provided helpful suggestions that led to improvements of the manuscript.

REFERENCES

Arakawa, A., and V. R. Lamb, 1981: A potential enstrophy- and energy-conserving scheme for the shallow water equations. *Mon. Wea. Rev.,* **109,** 18–36.

——, and Y.-J. G. Hsu, 1990: Energy conserving and potential-enstrophy dissipating schemes for the shallow water equations. *Mon. Wea. Rev.,* **118,** 1960–1969.

Borisov, S., and D. Nof, 1998: Deep, cross-equatorial eddies. *Geophys. Astrophys. Fluid Dyn.,* **87,** 273–310.

Choboter, P. F., and G. E. Swaters, 2000: Modeling equator-crossing currents on the ocean bottom. *Can. Appl. Math. Quart.,* **8,** 367–385.

Cushman-Roisin, B., 1994: *Introduction to Geophysical Fluid Dynamics.* Prentice Hall, 320 pp.

DeMadron, X. D., and G. Weatherly, 1994: Circulation, transport and bottom boundary layers of the deep currents in the Brazil Basin. *J. Mar. Res.,* **52,** 583–638.

Friedrichs, M. A. M., and M. M. Hall, 1993: Deep circulation in the tropical North Atlantic. *J. Mar. Res.,* **51,** 697–736.

Gent, P. R., and J. C. McWilliams, 1983: Consistent balanced models in bounded and periodic domains. *Dyn. Atmos. Oceans,* **7,** 67–93.

Hall, M. M., M. McCartney, and J. A. Whitehead, 1997: Antarctic Bottom Water flux in the equatorial western Atlantic. *J. Phys. Oceanogr.,* **27,** 1903–1926.

Hallberg, R., and P. Rhines, 1996: Buoyancy-driven circulation in an ocean basin with isopycnals intersecting the sloping boundary. *J. Phys. Oceanogr.,* **26,** 913–940.

Hsu, Y.-J. G., and A. Arakawa, 1990: Numerical modeling of the atmosphere with an isentropic vertical coordinate. *Mon. Wea. Rev.,* **118,** 1933–1959.

Jerlov, N. G., 1953: Studies of the equatorial currents in the Pacific. *Tellus,* **5,** 308–314.

Johnson, G. C., 1993: A deep inertial jet on a sloping bottom near the equator. *Deep-Sea Res.,* **40,** 1781–1792.

——, and J. M. Toole, 1993: Flow of deep and bottom waters in the Pacific at 10°N. *Deep-Sea Res.,* **40,** 371–394.

——, B. A. Warren, and D. B. Olson, 1991: Flow of bottom water in the Somali Basin. *Deep-Sea Res.,* **38,** 637–652.

Karsten, R. H., and G. E. Swaters, 1999: A unified asymptotic derivation of two-layer frontal geostrophic models including planetary sphericity and variable topography. *Phys. Fluids,* **11,** 2583–2597.

Matsuno, T., 1966: A finite difference scheme for time integrations of oscillatory equations with second order accuracy and sharp cut-off for high frequencies. *J. Meteor. Soc. Japan,* **44,** 85–88.

McCartney, M. S., and R. A. Curry, 1993: Transequatorial flow of Antarctic Bottom Water in the western Atlantic Ocean: Abyssal geostrophy at the equator. *J. Phys. Oceanogr.,* **23,** 1264–1276.

Nof, D., 1983: The translation of isolated cold eddies on a sloping bottom. *Deep-Sea Res.,* **30,** 171–182.

——, and S. Borisov, 1998: Inter-hemispheric oceanic exchange. *Quart. J. Roy. Meteor. Soc.,* **124,** 2829–2866.

Pedlosky, J., 1987: *Geophysical Fluid Dynamics.* 2d ed. Springer-Verlag, 710 pp.

——, 1996: *Ocean Circulation Theory.* Springer-Verlag, 453 pp.

Pickart, R. S., and R. X. Huang, 1995: Structure of an inertial deep western boundary current. *J. Mar. Res.,* **53,** 739–770.

Quadfasel, D., J. Fischer, F. Schott, and L. Stramma, 1997: Deep water exchange through the Owen Fracture Zone in the Arabian Sea. *Geophys. Res. Lett.,* **24,** 2805–2808.

Reszka, M. K., G. E. Swaters, and B. R. Sutherland, 2002: Instability of abyssal currents in a continuously stratified ocean with bottom topography. *J. Phys. Oceanogr.,* **32,** 3528–3550.

Rhein, M., L. Stramma, and U. Send, 1995: The Atlantic Deep Western Boundary Current: Water masses and transports near the equator. *J. Geophys. Res.,* **100,** 2441–2457.

Roemmich, D., S. Hautala, and D. Rudnick, 1996: Northward abyssal

transport through the Samoan Passage and adjacent regions. *J. Geophys. Res.,* **101,** 14 039–14 055.
Rudnick, D. L., 1997: Direct velocity measurements in the Samoan Passage. *J. Geophys. Res.,* **102,** 3293–3302.
Sandoval, F. J., and G. L. Weatherly, 2001: Evolution of the deep western boundary current of Antarctic Bottom Water in the Brazil Basin. *J. Phys. Oceanogr.,* **31,** 1440–1460.
Stephens, J. C., and D. P. Marshall, 2000: Dynamical pathways of Antarctic Bottom Water in the Atlantic. *J. Phys. Oceanogr.,* **30,** 622–640.
Stommel, H., and A. B. Arons, 1972: On the abyssal circulation of the World Ocean—V. The influence of bottom slope on the broadening of inertial boundary currents. *Deep-Sea Res.,* **19,** 707–718.
Swaters, G. E., 1991: On the baroclinic instability of cold-core coupled density fronts on a sloping continental shelf. *J. Fluid Mech.,* **224,** 361–382.
——, 1993: Nonlinear stability of intermediate baroclinic flow on a sloping bottom. *Proc. Roy. Soc. London,* **442A,** 249–272.
——, 1998: Numerical simulations of the baroclinic dynamics of density-driven coupled fronts and eddies on a sloping bottom. *J. Geophys. Res.,* **103,** 2945–2961.
——, and G. R. Flierl, 1991: Dynamics of ventilated coherent cold eddies on a sloping bottom. *J. Fluid Mech.,* **223,** 565–587.
Wijffels, S. E., J. M. Toole, H. L. Bryden, R. A. Fine, W. J. Jenkins, and J. L. Bullister, 1996: The water masses and circulation at 10°N in the Pacific. *Deep-Sea Res.,* **43,** 501–544.